Article

Copper Nanoplates for Printing Flexible High-Temperature Conductors

Aaron Sheng, Saurabh Khuje, Jian Yu,* Thomas Parker, Jeng-Yuan Tsai, Lu An, Yulong Huang, Zheng Li, Cheng-Gang Zhuang, Lanrik Kester, Qimin Yan, and Shenqiang Ren*

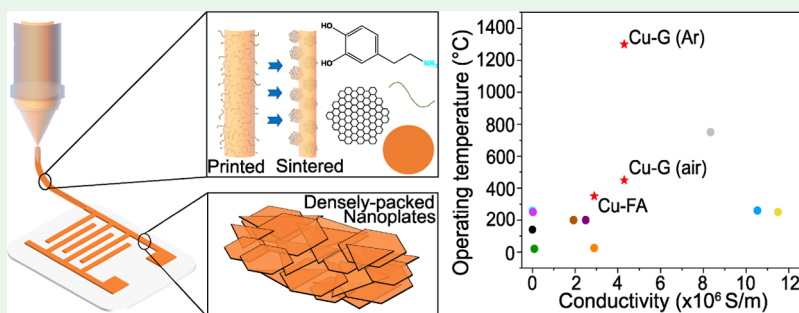Cite This: *ACS Appl. Nano Mater.* 2022, 5, 4028–4037

Read Online

ACCESS | Metrics & More | Article Recommendations | Supporting Information

ABSTRACT: Copper has attracted immense interest in advanced electronics attributed to its abundance and high electrical and thermal characteristics. However, the ease of oxidation when subjected to heat and humidity drastically limits its material reliability under extreme environments. Here, we utilize copper nanoplates as a building block to achieve a thermally stable (upwards of 1300 °C), antioxidation, and anticorrosion-printed conductor, with the capability of additively manufacturing on Corning flexible Alumina Ribbon Ceramic. We elucidate the printed copper nanoplates with a low sheet resistance of 4 mΩ/sq/mil by means of a surface-coordinated formate that inculcates high oxidation and corrosion resistance on a molecular level. In addition, an in situ copper–graphene conversion leads to a hybridized conductor displaying stability at elevated temperatures up to 1300 °C with high ampacity. Further mechanistic studies reveal high-temperature stability from in situ graphene conversion for copper and graphene interfaces, and preferential stacking of copper nanoplates, distinctly suited for emerging high-temperature flexible electronics.

KEYWORDS: *copper nanoplates, antioxidation, anticorrosion, high temperature, advanced electronics*

INTRODUCTION

Advanced electronics are undergoing a paradigm shift to increase their printability, portability, miniaturization, and versatility in different environments.[1-5] Simultaneously, electrical conducting materials, like metals, must complement the shift toward reliable, highly resistant, and high-performance conductors under extreme environments such as high temperatures and in reactive atmospheres.[6] Achieving such disparate functionalities will require the rational design and manufacturing of the conductor material and its hierarchical structures. However, traditional metal conductors are energetically expensive to produce and are susceptible to extreme environments,[5] creating a challenge for next-generation flexible electronic applications.[7] Printable electronics, on the other hand, allow miniaturizing of electronic devices to be increasingly versatile and portable. However, the difficulties lie in the nanoscaled materials used, where the higher surface-to-volume ratios lead to lower melting points and greater susceptibility to oxidation and corrosion, relative to their bulk counterparts.[8-10] In addition, the two most common types of conductors have diametrically opposite properties: higher melting point with lower conductivities (e.g., tungsten and nickel) and lower melting points with higher conductivities (e.g., silver and gold).

One promising metal conductor is copper, a ubiquitous electrically conductive material used in electronics, with high conductivities and a melting point higher than most other highly conductive metals,[1,9,10] and is significantly more abundant and inexpensive. However, a rudimentary issue with bulk copper materials is their high susceptibility to oxidation under ambient conditions.[11] Despite the success of utilizing energetically expensive fabrication of copper conductors through electroplating[8,12] or alloying,[2,3,8,9] printable copper conductors with the controlled feature dimensions have been highly sought after.[3,4,13,14] As such, there is a need for
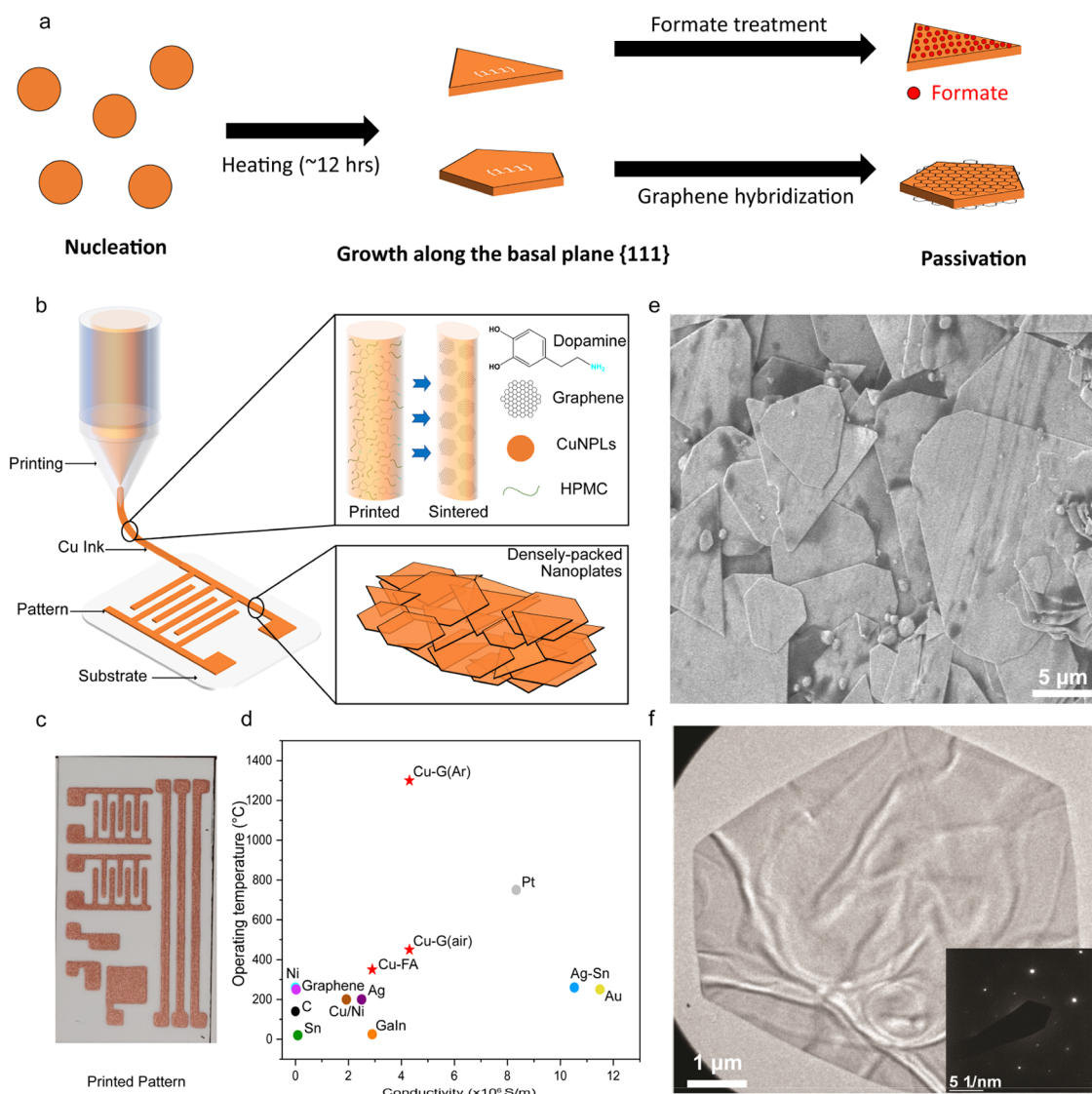
Figure 1. Copper nanoplates and their performance of printed Cu conductors. (a) A schematic of the synthesis of Cu NPLs from nucleation followed by surface passivation. (b) A schematic depicting the process of obtaining printed conductors. The HPMC is burned off during sintering, and the dopamine converts into graphene. (c) The image shows the final product of the printed sample. (d) Ashby plot of the operating temperature vs conductivity for different printable inks, which have been investigated (Pt,[44] GaIn,[45] Au,[46] Sn,[47] Cu/Ni,[48] graphene,[49] Ag−Sn[50]) or is commercially available (Ag,[51] C,[51] Ni[51]). The red stars are printed conductors discussed in this work. (e) SEM and (f) TEM images of a Cu NPL. The (f, inset) selected area electron diffraction (SAED) pattern of Cu NPL from panel (f).

developing a new printable conductive material with amplified electric performance and stability.[15] Printable copper conductors consist of nanostructured materials made from either nanoparticles, nanowires (1D), or nanoplates (2D). Copper nanoparticles (Cu NP) have been widely studied due to their facile synthesis,[16,17] whereas copper nanowires (Cu NWs) and copper nanoplates (Cu NPLs) are interesting due to their anisotropic growth, which provides a unique advantage over Cu NP. When compared to Cu NPs, Cu NWs have significantly lower percolation thresholds for a conductive film due to high aspect ratios of the nanostructure. This allows for NWs to be utilized in applications like wearable electronics[18−20] or as transparent conductive oxides (TCOs).[21,22] Cu NPLs, on the other hand, have a percolation threshold that is between that of Cu NPs and Cu NPLs. Once percolated, however, Cu NPLs show great potential due to higher ampacity[10] and electromagnetic interference shielding capabilities[23] from plate stacking as a result of their 2D

architecture. The printability of the conductive inks is also of great importance. Cu NPs have the best printability due to smaller sizes but can have potential issues with agglomeration of the NPs, which can result in fragile prints.[24] In addition to these, Cu NWs tend to suffer from clogging of the nozzles due to the large aspect ratio, thus limiting the available printing techniques.[1,2,20] Cu NPLs, due to the 2D architecture, do not suffer from nozzle clogging as much from the larger aspect ratio but are limited to the size of the basal plane (similar to the diameter of Cu NPs).

Past the basic conductive ink, passivation and sintering of the conductor are most likely required. First, as mentioned before, copper is easily oxidized and requires passivation to protect the surface. This can be achieved through a variety of methods such as molecular passivation,[25] core/shell passivation,[8,26,27] and polymer encapsulation[28,29] to name a few. Second, most conductive inks require an additive that must be decomposed via sintering for a better connection between
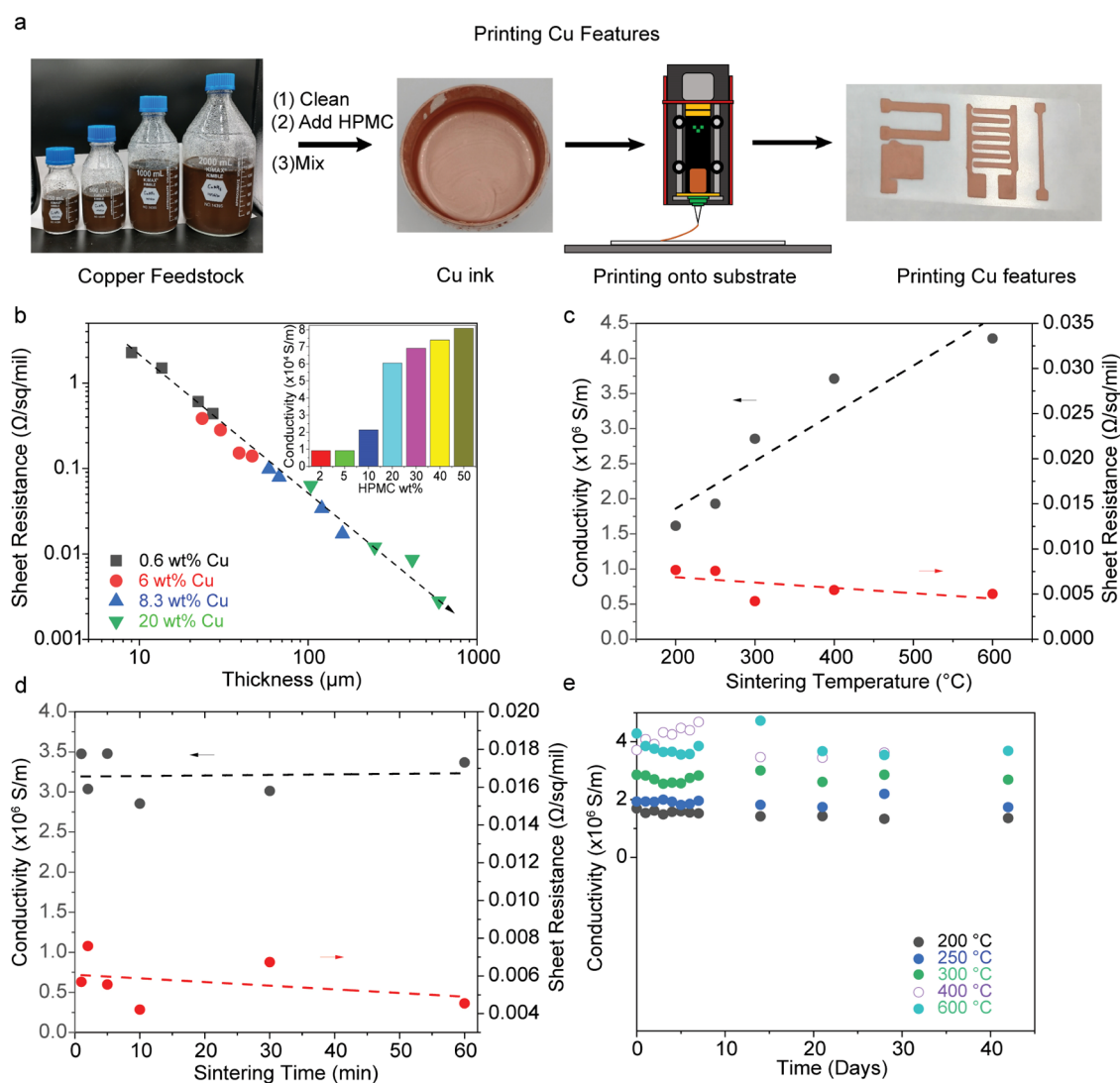
Figure 2. Electronic characteristics of printed copper features under processing conditions. (a) The process of printing Cu features, starting from the feedstock, to Cu ink preparation, to printing, and lastly drying the printed Cu testing or sintering. (b) Sheet resistance dependence on the thickness of the conductive print. Varying thickness was dependent on the number of printing passes and the Cu wt % in the ink. The inset shows the effects of HPMC concentration on the conductivity of the prints. The conductivity and sheet resistance values of printed Cu NPLs at varying sintering temperatures (c) and times (d). (e) Overtime conductivity of sintered prints for 42 days.

percolated nanostructures. Two common techniques used for sintering conductors involve photonic sintering[30,31] and thermal sintering in a tube furnace.[1,2,20,23] Both techniques require high temperatures to decompose the additives, but photonic sintering requires pulsed light and can be done in ambient conditions, whereas the tube furnace relies on conventional heating and requires inert gas to protect from oxidation.

In this study, we describe the controlled growth and hybridization strategies of the 2D highly crystalline copper (111) nanoplate (Cu NPL) morphology as a building block (Figure 1a) for the development of high-temperature stability, antioxidation, and anticorrosion conductor materials, with the capability of additive manufacturing onto Corning flexible Alumina Ribbon Ceramic[32] (Figure 1b). We emphasize that the surface coordination of formate could introduce high oxidation and corrosion resistance[25] for the printed Cu conductors (Cu-FA) without influencing their electrical conductivity (a sheet resistance of 4 mΩ/sq/mil), in addition to the increased working temperature by 100 °C compared to

that of untreated Cu conductors. We also utilized an in situ copper−graphene (Cu−G) conversion,[1] with the resulting conductors demonstrating stability at high temperatures, surviving up to 1300 °C (Figure 1c). This improved stability and conductivity at elevated temperatures are a result of the electronic hybridization between copper and graphene interfaces, which is supported by molecular dynamic simulations and in situ spectroscopies. Lastly, further characterizations were made to determine the purity of the Cu NPLs in addition to their stacking orientation. The developed Cu NPL ink for printed conductors, along with the demonstrated additive manufacturing process, is promising for electronic applications where specific geometric patterning is required.

■ RESULTS AND DISCUSSION

The overall scheme starting with the synthesis of the Cu NPLs, following the passivation of these NPLs, is shown in Figure 1a. Figure 1b illustrates the schematic of the fabrication process utilized for printing the Cu ink (illustration of Figure 1b
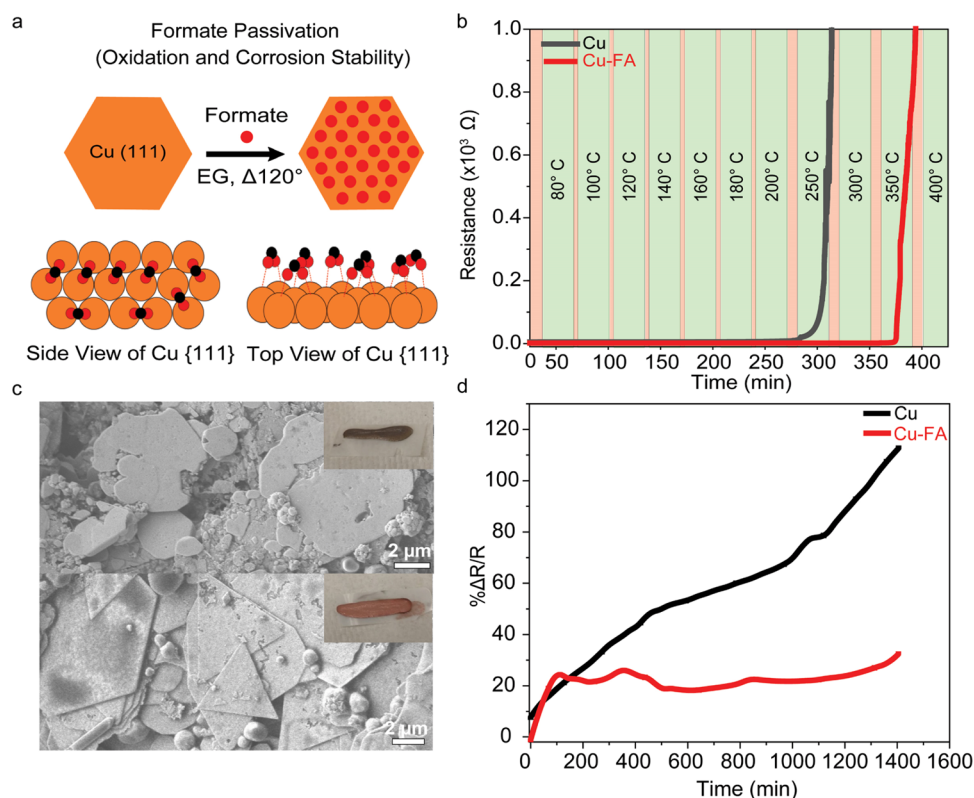
Figure 3. Anticorrosion and antioxidation performance of Cu NPLs and Cu NPL-FA conductors. (a) Hybridizing strategy: formate passivation of the Cu {111} facet. A model of Cu NPLs with formate molecules passivating the surface. (b) Oxidation resistance study of bare Cu NPLs (black) vs Cu NPL-FA (red) at increasing temperatures. The red boxes represent the temperature ramping up at 5 °C/min. The green boxes represent the holding temperature specified for 30 min. (c) The SEM images (left) of Cu NPLs (top) and Cu NPL-FA (bottom) after base corrosion testing. The insets are images of the Cu prints after. The resistance change (d) of the Cu prints during prolonged submersion in a 0.1 M NaOH solution.

depicts the example of the in situ conversion of dopamine to graphene in the Cu−G conductor). Figure 1c shows the printed pattern on an Alumina Ribbon Ceramic substrate. The electrical conductivities of various Cu-based conductors (presented here from commercial sources) and their respective operating temperatures are shown in an Ashby plot (Figure 1d). Our Cu-hybridized conductors are observed to have not only higher operating temperatures than most of the printable inks but also higher electrical conductivities. Interestingly, Cu−G in an inert atmosphere is shown to have the highest operation temperature, even above the melting point of bulk copper. It should be noted that the only printable inks with higher electrical conductivities are comprised of noble metals.

Anisotropic Growth of Copper Nanoplates. The dimension/shape control of copper nanostructures is a fundamental component in the development of printable conductive ink material, as size limits the printing technique used.[33] For the synthesis of Cu NPLs, one method that has been explored was by introducing iodide in the reaction mixture.[10,34] Lee et al. utilized a simple hydrothermal synthesis method to synthesize Cu NWs and Cu NPLs just by adding iodide. By utilizing the wet-chemistry synthesis, we showed controlled growth of 2D highly crystalline Cu NPLs through the reduction of copper chloride by glucose and subsequent adsorption of iodide on the Cu (111) plane (Figures S1 and S2). It should be noted that iodide also adsorbs on the (100) plane as well and also increases the rate of growth on that plane.[34] The iodine adsorption on the (111) plane acts as a

shape-directing agent where it hinders the growth on the (111), resulting in an anisotropic growth in the 2D direction.[34]

The addition of hexadecylamine (HDA) acts mainly as a ligand and a main component in forming the penta-twinned Cu seeds.[35] Its long chain also allows for tightly packed monolayers that prevent aggregation and also protection for the copper from oxidizing. HDA also plays a large role in the growth of Cu NWs. However, HDA is only physisorbed on the copper, not contributing to the growth of the Cu NPLs themselves. The scanning and transmission electron microscopic (SEM and TEM) images of as-synthesized Cu NPLs are shown in Figure 1e,f, revealing the 2D architecture of as-synthesized ultrathin Cu NPLs.

Here, we define our 2D plate morphology (Cu NPLs) as having an aspect ratio between the basal plane and thickness to be greater than 10. The selected area electron diffraction (SAED) pattern (Figure 1f, inset) for the Cu NPLs in Figure 1f suggests their highly crystalline nature. In addition, the hexagonal diffraction pattern is an indication that the basal plane is the Cu {111} facet. The size distribution of synthesized Cu NPLs can be well controlled by manipulating the nucleation and growth by means of tuning the reaction conditions discussed in the Supporting Information (Figure S1b−d).

Physical Characteristics of Cu NPL Conductors. The observations above described the controlled synthesis of printable Cu material feedstocks for the development of an aqueous-based ink material to be printed for the evaluation of its electrical conductivity (Figure 2a).

Effect of Thickness and HPMC Concentration on the Conductivity of Printed Cu Conductor. Figure 2b shows the relationship between the sheet resistance and Cu loading concentrations of the printed features, where the increase of Cu concentration (wt %) and the number of printing passes increases the thickness of the printed feature. Furthermore, the increase in thickness also correlates with the decrease in its sheet resistance. Ideally, a low sheet resistance could be achieved at a higher Cu feedstock; however, the Cu ink's printability becomes increasingly difficult at feedstock concentrations above 6 wt %. Additionally, on a linear scale (Figure S3a), the decrease in sheet resistance becomes minor once the thickness reaches above 50 μm. Therefore, a 6 wt % Cu feedstock is selected for the following studies.

In addition, the inset of Figure 2b describes the electrical conductivity dependence on the hydroxypropyl methylcellulose (HPMC) additive concentration for printed Cu features for tuning viscosity and printability. The electrical conductivity increases from 1×10^3 to 8×10^3 S/m, an 8-fold increase, by increasing the HPMC solution content from 2 to 50 wt % in the copper ink. The increased conductivity is a result of an improved adhesion and dispersibility of Cu in the preparation of the printable ink materials.[24] The electrical conductivity improved most significantly from 10 to 20 wt % HPMC in the printable Cu materials (from 2×10^3 to 6×10^3 S/m), while any further increase in HPMC above 20 wt % shows minor increments in the conductivity. Therefore, 20 wt % HPMC is selected for further studies.

Electrical Conductivity of Sintered Cu NPLs at Different Sintering Conditions and Overtime Stability. To further increase its conductivity (or decrease the sheet resistance), a postsintering treatment for the printed Cu patterns is crucial. Sintering results in the improvement of the conductivity/lower sheet resistance through the decomposition of nonconductive organics while annealing the Cu nanostructures for increased contact and density.[1] By varying the sintering temperature (Figure 2c) from 200 to 600 °C, a clear trend is observed, indicating an increased conductivity from 1.5×10^6 to 4.2×10^6 S/m. In addition, the most significant increase of electrical conductivity occurs at a sintering temperature from 250 to 300 °C, which correlates to the heating curve in Figure S4 (discussion in the Supporting Information).

However, there is no significant difference past 300 °C. When investigating the effects of sintering time from 1 to 60 min (Figure 2d) at 300 °C, no trend is observed and that electrical conductivities varied from 3×10^6 to 3.5×10^6 S/m. In addition, the stability of the printed copper features in ambient conditions (Figure 2e) is measured over a duration of 42 days. The printed Cu patterns show little to no change in their conductivity over that time span, demonstrating high stability in ambient conditions.

Formate Passivation Strategy. Copper nanostructures' lower resistance to oxidation and corrosion is due to their high surface-to-volume ratio, compared to bulk copper.[36,37] Improving their antioxidation and anticorrosion properties is vital in prolonging the lifetime and electrical performance of printed Cu features. Here, we describe a surface hybridization strategy by introducing formates (FA) onto the printed highly crystalline Cu (111) NPLs (Figure 3a). The surface passivation occurs with FA binding to neighboring copper atoms at the surface.[38] Through this Cu-FA hybridization, we demonstrate the enhancement in oxidation resistance of Cu conductors.[25]

Improved Thermal Stability of Formate-Treated Cu NPL Conductors. Figure 3b compares the oxidation resistance between Cu and Cu-FA under ambient conditions at increased temperatures. Both conductors survive oxidation at 200 °C; however, the Cu conductor starts oxidizing significantly at 250 °C. The Cu-FA conductor, on the other hand, oxidizes at 350 °C, an increased working temperature of about 100 °C, compatible with the maximum working temperature of flexible polymer substrates, like Kapton. The increased oxidation resistance of Cu-FA can be attributed to the surface formate layer, preventing oxygen from oxidizing the Cu surface.[38] At 350 °C, however, the surface formate layer decomposes, exposing and subsequently allowing oxygen on the conductor surface. In addition to the enhanced oxidation resistance, the Cu-FA hybridization also enhances the corrosion resistance.[38]

Improved Corrosion Stability of Formate-Treated Cu NPL Conductors. The SEM images (Figure 3c) are shown of Cu (top) and Cu-FA (bottom) after prolonged base treatment, in which a pronounced corrosion and surface reconstruction can be observed on the Cu conductor. This surface reconstruction on the Cu conductor was the direct result of forming oxides on the copper surface. This breaks down while also disfiguring the sharpness of the NPLs. In addition, oxidation can also result in voids formed in the Cu NPLs. On the other hand, Cu-FA conductors retain their distinct shapes, with little to no visible damage to the printed structure. The insets for each SEM image (Figure 3c) correspond to the image after the base treatment. The measured resistances under base corrosion measurement (Figure 3d) of Cu and Cu-FA reveal the anticorrosion nature for Cu-FA, with no significant resistance change. Cu-FA shows an increasing trend for the first 100 min; however, the resistance plateaus remain steady. Cu, however, shows a steady increase in resistance over time.

Additionally, cyclic voltammetry was performed to evaluate the Cu oxidation stability. Cu-FA shows a stable voltammogram, whereas the voltammogram of Cu NPLs shifts and varies between runs (further discussion is shown in the Supporting Information). These observations help support the superior stability of Cu-FA toward anticorrosion. These observations suggest the enhanced antioxidation and anticorrosion performance of surface-hybridized Cu conductor through the formate passivation.

Copper–Graphene Hybridization Strategy for High-Temperature Stability. The use of graphene in metal composites has shown to provide interesting benefits, like thermal stability,[1,39] improved ampacity,[40] improved corrosion resistance, and improved electrical conductivity of copper.[39] Here, we introduce an in situ direct conversion of molecular dopamine and hybridization strategy of Cu–graphene conductors focusing on extreme environments such as high temperatures, where the temperatures greatly exceed 1084 °C (bulk copper's melting point). The in situ Cu–G direct conversion is achieved through dopamine coating during the Cu ink preparation, which, when carbonized at elevated temperatures, serves as a potential graphene source. This can be attributed to the presence of hydroxyl (−OH) and amine (−NH$_2$) groups forming a uniform coating on the Cu nanoplate surface, which, in turn, is attributed to their strong adhesion due to noncovalent bonds (hydrogen bonding or $\pi-\pi$ stacking), resulting in the enhancement of electrical conductivity due to metallic and covalent bond formation between the graphene and copper (111) nanoplates. Once sintered, the resulting conductor has a high conductivity (4.3 ×
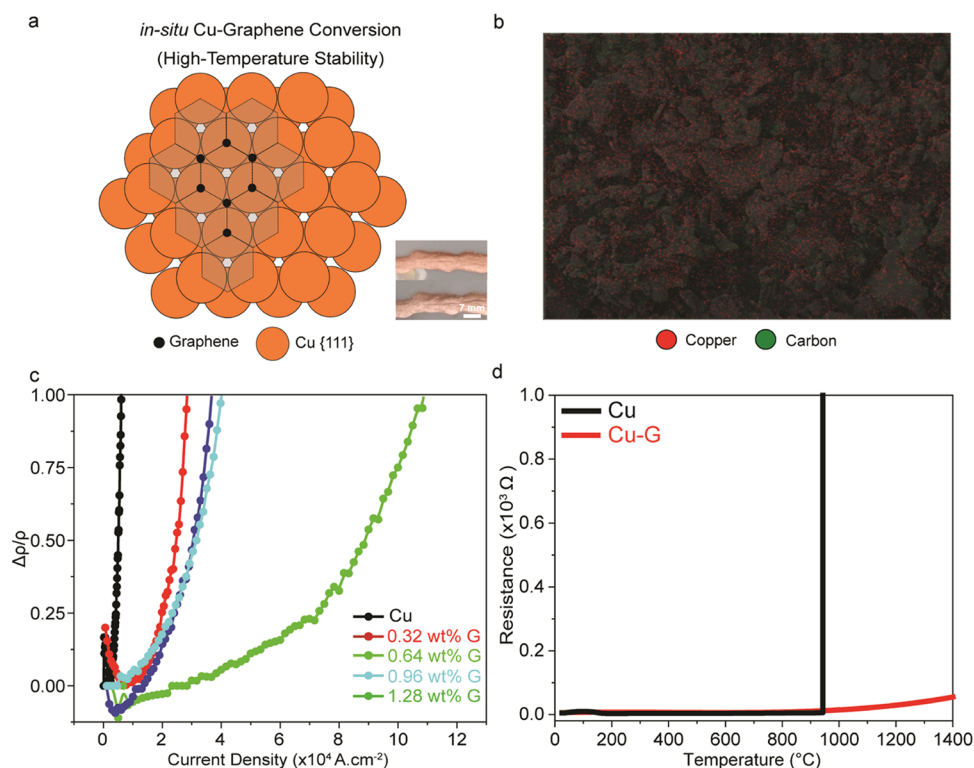
Figure 4. Ampacity and high-temperature electric performance of printed Cu−G conductors. (a) Hybridizing strategy: graphene formation onto the Cu {111} facet. A model of how graphene stacks on top of the Cu {111} facet after heating at 1300 °C. The inset image shows the Cu prints before (top) and after (bottom) sintering at 1300 °C. (b) A SEM image of Cu−G NPLs after surviving up to 1300 °C. (c) Ampacity measurements for pure Cu NPLs and Cu−G at various dopamine concentrations (0.32−1.28 wt % G). (d) Resistance change measurement at increasing temperatures of Cu NPLs (black) and Cu−G NPLs (red).

10^6 S/m). The Raman spectrum and XRD diffractograms help support the formation of the graphene and the quality of the conductor (Figure S9). A model depicts how the graphene layer preferentially adsorbs onto the Cu {111} facet (Figure 4a), effectively passivating and hybridizing the Cu conductor. The adjoined images (Figure 4a, inset) show the printed Cu feature before (top) and after (bottom) sintering, showing no signs of melting after sintering up to 1400 °C, significantly above the bulk copper's melting point.

Improved Ampacity and Thermal Stability of Cu−G Hybridized Conductor. A SEM and energy-dispersive X-ray spectroscopic image (Figure 4b) shows the printed Cu feature after sintering, revealing the uniform distribution of Cu and C elements. X-ray diffraction (XRD) is used (Figure S9b) to characterize the Cu−G conductors after heating up to 1400 °C. The three peaks observed at 2θ values at 43.3, 50.5, and 74.1° are characteristic for Cu (FCC), corresponding to {111}, {200}, and {220} planes, respectively. The intense peak related to the Cu {111} lattice plane suggests that the Cu (111) is maintained, further suggesting that the printed Cu−G conductors have survived after sintering at 1400 °C. Figure 4c shows the ampacity measurements between pure Cu NPLs and Cu−G conductors. Varying dopamine concentrations reveal an increase in ampacity from pure Cu NPLs to 0.64 wt % G followed by a decrease in ampacity at 0.96 and 1.28 wt % G, suggesting that 0.64 wt % G is the optimal concentration. Cu−G (0.64 wt %), when compared to pure Cu NPLs, shows an increase of ∼20-fold (approximately from 0.5×10^4 to 10×10^4 A·cm^{-2}) in the current-carrying capacity, which assists in concluding that electric and thermal conductivities of the Cu−G conductor are remarkably higher compared to those of Cu

NPLs, which further accentuates the role of graphene on high-temperature stability and thus reliability. The role of graphene in improving the ampacity of the Cu−G conductors is due to the high thermal conductivities of graphene. In addition, high-temperature conductivity studies (Figure 4d) are performed, comparing the printed Cu NPLs and Cu−G features sintered under an inert atmosphere up to 1400 °C, whereas printed Cu NPLs failed around 950 °C. Both the enhanced performances observed can be attributed to the graphene's role in suppressing Cu diffusion and its high thermal conductivity and hybridizing Cu and graphene at the interface during in situ conversion. In addition to its high-temperature performance, we also demonstrate graphene's ability to enhance the anticorrosion properties of Cu and to significantly suppress Cu diffusion through preferential lattice matching. In addition, we tested its anticorrosion properties (Figure S10; discussion in the Supporting Information).

Simulation of Copper−Graphene Interaction at Elevated Temperatures. To understand the effects of graphene incorporation in copper on its bonding behavior of alloy systems, we performed molecular dynamic simulations for a pristine copper system including six atomic layers along the [001] direction and a copper−graphene−copper heterogeneous structure with temperatures at 800 K (Figure S12), 1200 K (Figure S13), 1600 K (sintered, Figure 5a; unsintered, Figure S11), and 2000 K (Figure S14). We observed that large atomic displacements of copper atoms away from their equilibrium positions in a pristine 6-layer copper slab appear at around 1200 K and are enhanced when the temperature is increased up to 2000 K. On the other hand, copper atoms in the copper−graphene−copper heterogeneous structure exhibit
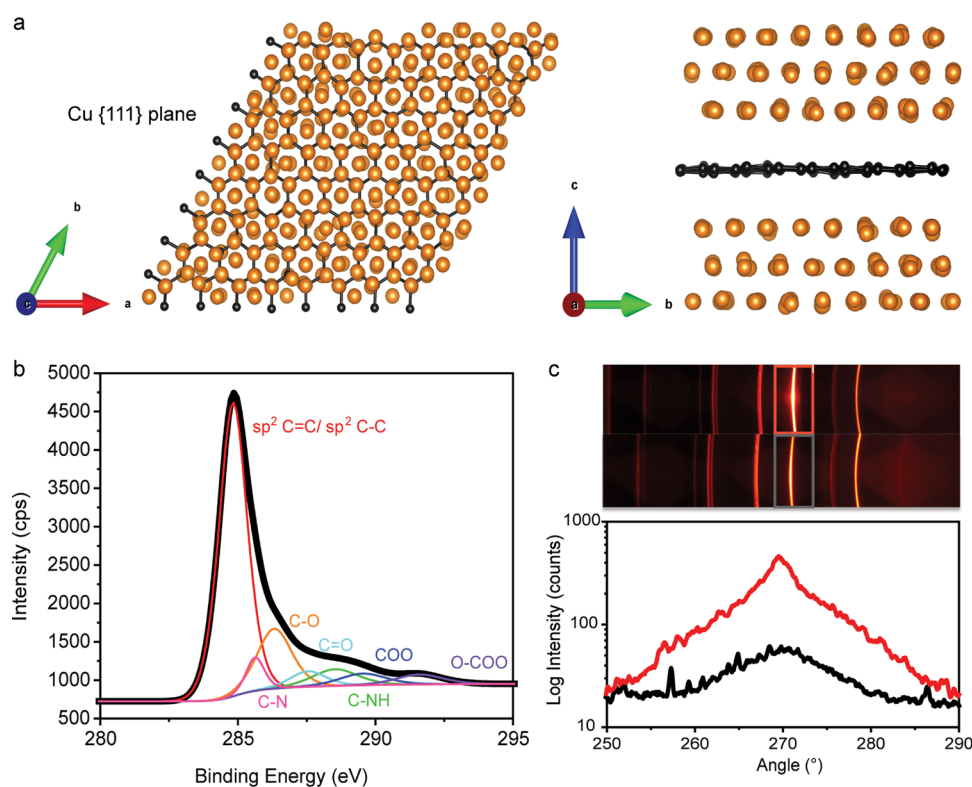
Figure 5. Mechanistic studies of Cu−G conductors through theoretical modeling and spectroscopy. (a) Molecular dynamics simulations of a copper−graphene−copper heterogeneous structure at 1600 K at top-down (left) and side views (right). (b) The XPS spectrum of the sintered Cu−G at the carbon core (C 1s) region. The region has been deconvolved into several peaks depicting different chemical environments, with residuals suggesting a good fit. (c) The 2D XRD scans (top) and the corresponding XRD crystal tilt orientation study at a 2θ value of 43.3° (red, sintered; gray, unsintered). The graph (bottom) shows the average crystal tilt of unsintered (black) and sintered (red) Cu−G prints.

much less deviations from their equilibrium positions. The results provide strong evidence that the incorporation of graphene is able to enhance the bonding stability of the whole structure at higher temperatures and hence increase the melting point of the system.

XPS Investigation of Sintered (and Unsintered) Cu−G Conductors. X-ray photoelectron spectroscopy (XPS) can be utilized in determining the present elements and their chemical environments of printed Cu−G conductors (Figure S15). Figure 5b shows the XPS spectrum of the sintered Cu−G sample with six clearly different chemical environments around 284.87, 286.21, 288.51, 287.42, 289.54, and 291.27 eV corresponding to sp^2 and sp^3 carbons, C−O, C−NH$_x$, C═O, COO, and O−COO functional groups, respectively (the XPS of unsintered Cu−G and various other environments is shown and discussed in the Supporting Information).[41,42] To further support the in situ conversion of dopamine to graphene, the N 1s XPS spectrum (Figure S18) was investigated. The unsintered sample showed one peak at 399.61 eV, which corresponds to pyridinic/pyrrolic N. Once sintered, an additional peak appeared at 401.00 eV corresponding to graphitic N, indicating the successful formation of the nitrogen-doped graphene of the printed Cu−G conductor.[43] The XPS data have clearly shown that printed Cu conductors are purely metallic, before and after sintering, as well as confirming the presence and conversion of polydopamine to nitrogen-doped graphene.

Stacking Orientation of Cu−G Conductors. In addition to interpreting the X-ray diffraction pattern of Cu−G conductors (Figure S9), crystal tilt orientation can tease out information regarding how the Cu NPLs are stacking. Mapping the crystal tilt (Figure 5c) for the (111) plane (43.3°) in both sintered and unsintered prints, there is a relatively broad spectrum with the peak intensity at 270°, corresponding to the sample normal. The anisotropy in the Debye ring indicates the preferential orientation of the Cu NPLs, with narrower peaks suggesting that the alignment between the Cu NPLs is increasing. The corresponding FWHMs for the sintered and unsintered prints are 4 and ~10°, respectively, suggesting that once sintered, the Cu NPLs are oriented in roughly the same direction and preferentially stacked on top of one another.

■ CONCLUSIONS

In this study, we report highly crystalline Cu (111) nanoplates as the building block for the development of antioxidation Cu conductors with high conductivity and stability under extreme environments. We describe two hybridization strategies for printed Cu conductors: one involving formate passivation to show antioxidation and anticorrosion and the other with the in situ conversion of dopamine to graphene, displaying remarkable stability at high temperatures (1400 °C), exceeding the melting point of bulk copper (1084 °C). The printed Cu conductors display a high electric conductivity of 4×10^6 S/m and a sheet resistance of 4 mΩ/sq/mil, which can be printed onto a variety of flexible substructures, including high-temperature Kapton plastics and flexible Alumina Ribbon Ceramic substrates. The Cu−G conductor displays an ~20-fold increase in the current-carrying capacity when directly compared with the Cu conductor. Additionally, its high-temperature stability was computationally modeled. The

findings shown here represent a new conductor material building block and promising strategies to address the material's reliability issues for printed electronics at high temperatures. These observations depict that our hybridized Cu NPL conductors featuring antioxidation and anticorrosion properties and stability at elevated temperatures deem them suitable for a plethora of printed miniaturized electronic applications. Moreover, the size, ease of manufacturing, and scalability make them excellent candidates for advanced electronics.

■ ASSOCIATED CONTENT

Ⓢ Supporting Information

The Supporting Information is available free of charge at https://pubs.acs.org/doi/10.1021/acsanm.2c00019.

> Control of copper nanoplates, molecular formula and structure of printed copper materials, SEM image of printed copper on Alumina Ribbon Ceramic substrate after sintering, electric data comparison between copper and silver ink, Raman spectrum of substrate, and XPS and XRD results before and after sintering (PDF)

■ AUTHOR INFORMATION

Corresponding Authors

Jian Yu − Army Research Laboratory, Aberdeen Proving Ground, Maryland 21005, United States; Email: jian.h.yu.civ@army.mil

Shenqiang Ren − Department of Chemistry, University at Buffalo, The State University of New York, Buffalo, New York 14260, United States; Department of Mechanical and Aerospace Engineering, Research and Education in Energy Environment & Water Institute and Research and Education in Energy Environment & Water Institute, University at Buffalo, The State University of New York, Buffalo, New York 14260, United States; ⓞ orcid.org/0000-0002-9987-3316; Email: shenren@buffalo.edu

Authors

Aaron Sheng − Department of Chemistry, University at Buffalo, The State University of New York, Buffalo, New York 14260, United States; ⓞ orcid.org/0000-0003-0342-6456

Saurabh Khuje − Department of Mechanical and Aerospace Engineering, Research and Education in Energy Environment & Water Institute, University at Buffalo, The State University of New York, Buffalo, New York 14260, United States

Thomas Parker − Army Research Laboratory, Aberdeen Proving Ground, Maryland 21005, United States

Jeng-Yuan Tsai − Department of Physics, Temple University, Philadelphia, Pennsylvania 19122, United States

Lu An − Department of Mechanical and Aerospace Engineering, Research and Education in Energy Environment & Water Institute, University at Buffalo, The State University of New York, Buffalo, New York 14260, United States

Yulong Huang − Department of Mechanical and Aerospace Engineering, Research and Education in Energy Environment & Water Institute, University at Buffalo, The State University of New York, Buffalo, New York 14260, United States; ⓞ orcid.org/0000-0002-9616-0134

Zheng Li − Department of Mechanical and Aerospace Engineering, Research and Education in Energy Environment & Water Institute, University at Buffalo, The State University of New York, Buffalo, New York 14260, United States; ⓞ orcid.org/0000-0002-1218-2927

Cheng-Gang Zhuang − Corning Research and Development Corporation, Corning, New York 14830, United States

Lanrik Kester − Corning Research and Development Corporation, Corning, New York 14830, United States

Qimin Yan − Department of Physics, Temple University, Philadelphia, Pennsylvania 19122, United States

Complete contact information is available at:
https://pubs.acs.org/10.1021/acsanm.2c00019

Author Contributions

The manuscript was written through contributions of all authors. S.R. and J.Y. designed and supervised the project. A.S. and S.K. worked on the synthesis of Cu nanostructures and the printable ink preparation. T.P. and J.Y. carried out the XPS and XRD studies. J.-Y.T. and Q.Y. worked on the modeling studies, and C.-G.Z. and L.K. studied the flexible Alumina Ribbon Ceramic. L.A., Y.H., and Z.L. worked on the structural characterization.

Notes

The authors declare no competing financial interest.
All data needed to evaluate the conclusions are present in this paper and/or the Supporting Materials.

■ ACKNOWLEDGMENTS

■ REFERENCES

(1) Li, Z.; Khuje, S.; Chivate, A.; Huang, Y.; Hu, Y.; An, L.; Shao, Z.; Wang, J.; Chang, S.; Ren, S. Printable Copper Sensor Electronics for High Temperature. ACS Appl. Electron. Mater. 2020, 2, 1867−1873.

(2) Li, Z.; Scheers, S.; An, L.; Chivate, A.; Khuje, S.; Xu, K.; Hu, Y.; Huang, Y.; Chang, S.; Olenick, K.; Olenick, J.; Choi, J. H.; Zhou, C.; Ren, S. All-Printed Conformal High-Temperature Electronics on Flexible Ceramics. ACS Appl. Electron. Mater. 2020, 2, 556−562.

(3) Jason, N. N.; Wang, S. J.; Bhanushali, S.; Cheng, W. Skin inspired fractal strain sensors using a copper nanowire and graphite microflake hybrid conductive network. Nanoscale 2016, 8, 16596−16605.

(4) Jason, N. N.; Shen, W.; Cheng, W. Copper Nanowires as Conductive Ink for Low-Cost Draw-On Electronics. ACS Appl. Mater. Interfaces 2015, 7, 16760−16766.

(5) Jo, S.; Choo, S.; Kim, F.; Heo, S. H.; Son, J. S. Ink Processing for Thermoelectric Materials and Power-Generating Devices. Adv. Mater. 2019, 31, No. 1804930.

(6) Lakshminarayanan, V.; Sriraam, N. In The Effect of Temperature on the Reliability of Electronic Components, IEEE International Conference on Electronics, Computing and Communication Technologies (CONECCT), 2014; pp 1−6.

(7) Naghdi, S.; Rhee, K. Y.; Hui, D.; Park, S. J. A Review of Conductive Metal Nanomaterials as Conductive, Transparent, and

Flexible Coatings, Thin Films, and Conductive Fillers: Different Deposition Methods and Applications. *Coatings* **2018**, *8*, No. 278.

(8) Ye, S.; Stewart, I. E.; Chen, Z.; Li, B.; Rathmell, A. R.; Wiley, B. J. How Copper Nanowires Grow and How To Control Their Properties. *Acc. Chem. Res.* **2016**, *49*, 442−451.

(9) Tomotoshi, D.; Kawasaki, H. Surface and Interface Designs in Copper-Based Conductive Inks for Printed/Flexible Electronics. *Nanomaterials* **2020**, *10*, No. 1689.

(10) Lee, J.-W.; Han, J.; Lee, D. S.; Bae, S.; Lee, S. H.; Lee, S.-K.; Moon, B. J.; Choi, C.-J.; Wang, G.; Kim, T.-W. 2D Single-Crystalline Copper Nanoplates as a Conductive Filler for Electronic Ink Applications. *Small* **2018**, *14*, No. 1703312.

(11) Lee, Y.; Choi, J.-r.; Lee, K. J.; Stott, N. E.; Kim, D. Large-scale synthesis of copper nanoparticles by chemically controlled reduction for applications of inkjet-printed electronics. *Nanotechnology* **2008**, *19*, No. 415604.

(12) Miura, S.; Honma, H. Advanced copper electroplating for application of electronics. *Surf. Coat. Technol.* **2003**, *169−170*, 91−95.

(13) Zhang, Y.; Guo, J.; Xu, D.; Sun, Y.; Yan, F. Synthesis of Ultralong Copper Nanowires for High-Performance Flexible Transparent Conductive Electrodes: The Effects of Polyhydric Alcohols. *Langmuir* **2018**, *34*, 3884−3893.

(14) Gong, S.; Cheng, W. One-Dimensional Nanomaterials for Soft Electronics. *Adv. Electron. Mater.* **2017**, *3*, No. 1600314.

(15) Reuss, R. H.; Chalamala, B. R.; Moussessian, A.; Kane, M. G.; Kumar, A.; Zhang, D. C.; Rogers, J. A.; Hatalis, M.; Temple, D.; Moddel, G.; Eliasson, B. J.; Estes, M. J.; Kunze, J.; Handy, E. S.; Harmon, E. S.; Salzman, D. B.; Woodall, J. M.; Alam, M. A.; Murthy, J. Y.; Jacobsen, S. C.; Olivier, M.; Markus, D.; Campbell, P. M.; Snow, E. Macroelectronics: Perspectives on Technology and Applications. *Proc. IEEE* **2005**, *93*, 1239−1256.

(16) Gawande, M. B.; Goswami, A.; Felpin, F.-X.; Asefa, T.; Huang, X.; Silva, R.; Zou, X.; Zboril, R.; Varma, R. S. Cu and Cu-Based Nanoparticles: Synthesis and Applications in Catalysis. *Chem. Rev.* **2016**, *116*, 3722−3811.

(17) Crisan, M. C.; Teodora, M.; Lucian, M. Copper Nanoparticles: Synthesis and Characterization, Physiology, Toxicity and Antimicrobial Applications. *Appl. Sci.* **2022**, *12*, No. 141.

(18) Hong, I.; Lee, S.; Kim, D.; Cho, H.; Roh, Y.; An, H.; Hong, S.; Ko, S. H.; Han, S. Study on the oxidation of copper nanowire network electrodes for skin mountable flexible, stretchable and wearable electronics applications. *Nanotechnology* **2018**, *30*, No. 074001.

(19) Kim, D.; Kwon, J.; Jung, J.; Kim, K.; Lee, H.; Yeo, J.; Hong, S.; Han, S.; Ko, S. H. A Transparent and Flexible Capacitive-Force Touch Pad from High-Aspect-Ratio Copper Nanowires with Enhanced Oxidation Resistance for Applications in Wearable Electronics. *Small Methods* **2018**, *2*, No. 1800077.

(20) Khuje, S.; Sheng, A.; Yu, J.; Ren, S. Flexible Copper Nanowire Electronics for Wireless Dynamic Pressure Sensing. *ACS Appl. Electron. Mater.* **2021**, *3*, 5468−5474.

(21) Kim, W.-K.; Lee, S.; Hee Lee, D.; Hee Park, I.; Seong Bae, J.; Woo Lee, T.; Kim, J.-Y.; Hun Park, J.; Chan Cho, Y.; Ryong Cho, C.; Jeong, S.-Y. Cu Mesh for Flexible Transparent Conductive Electrodes. *Sci. Rep.* **2015**, *5*, No. 10715.

(22) Cheng, Y.; Wang, S.; Wang, R.; Sun, J.; Gao, L. Copper nanowire based transparent conductive films with high stability and superior stretchability. *J. Mater. Chem. C* **2014**, *2*, 5309−5316.

(23) Choi, H. K.; Lee, A.; Park, M.; Lee, D. S.; Bae, S.; Lee, S.-K.; Lee, S. H.; Lee, T.; Kim, T.-W. Hierarchical Porous Film with Layer-by-Layer Assembly of 2D Copper Nanosheets for Ultimate Electromagnetic Interference Shielding. *ACS Nano* **2021**, *15*, 829−839.

(24) Yokoyama, S.; Nozaki, J.; Motomiya, K.; Tsukahara, N.; Takahashi, H. Strong adhesion of polyvinylpyrrolidone-coated copper nanoparticles on various substrates fabricated from well-dispersed copper nanoparticle inks. *Colloids Surf., A* **2020**, *591*, No. 124567.

(25) Peng, J.; Chen, B.; Wang, Z.; Guo, J.; Wu, B.; Hao, S.; Zhang, Q.; Gu, L.; Zhou, Q.; Liu, Z.; Hong, S.; You, S.; Fu, A.; Shi, Z.; Xie, H.; Cao, D.; Lin, C.-J.; Fu, G.; Zheng, L.-S.; Jiang, Y.; Zheng, N.

(26) Tigan, D.; Genlik, S. P.; Imer, B.; Unalan, H. E. Core/shell copper nanowire networks for transparent thin film heaters. *Nanotechnology* **2019**, *30*, No. 325202.

(27) Stewart, I. E.; Ye, S.; Chen, Z.; Flowers, P. F.; Wiley, B. J. Synthesis of Cu−Ag, Cu−Au, and Cu−Pt Core−Shell Nanowires and Their Use in Transparent Conducting Films. *Chem. Mater.* **2015**, *27*, 7788−7794.

(28) Kim, D.; Bang, J.; Lee, W.; Ha, I.; Lee, J.; Eom, H.; Kim, M.; Park, J.; Choi, J.; Kwon, J.; Han, S.; Park, H.; Lee, D.; Ko, S. H. Highly stretchable and oxidation-resistive Cu nanowire heater for replication of the feeling of heat in a virtual world. *J. Mater. Chem. A* **2020**, *8*, 8281−8291.

(29) Hong, I.; Roh, Y.; Koh, J.-S.; Na, S.; Kim, T.; Lee, E.; An, H.; Kwon, J.; Yeo, J.; Hong, S.; Lee, K.-T.; Kang, D.; Ko, S. H.; Han, S. Semipermanent Copper Nanowire Network with an Oxidation-Proof Encapsulation Layer. *Adv. Mater. Technol.* **2019**, *4*, No. 1800422.

(30) Park, J. H.; Han, S.; Kim, D.; You, B. K.; Joe, D. J.; Hong, S.; Seo, J.; Kwon, J.; Jeong, C. K.; Park, H.-J.; Kim, T.-S.; Ko, S. H.; Lee, K. J. Plasmonic-Tuned Flash Cu Nanowelding with Ultrafast Photochemical-Reducing and Interlocking on Flexible Plastics. *Adv. Funct. Mater.* **2017**, *27*, No. 1701138.

(31) Han, S.; Hong, S.; Ham, J.; Yeo, J.; Lee, J.; Kang, B.; Lee, P.; Kwon, J.; Lee, S. S.; Yang, M.-Y.; Ko, S. H. Fast Plasmonic Laser Nanowelding for a Cu-Nanowire Percolation Network for Flexible Transparent Conductors and Stretchable Electronics. *Adv. Mater.* **2014**, *26*, 5808−5814.

(32) Zhuang, et al. Flexibility matters: High purity, thin, flexible alumina ribbon ceramic. *Ceramic & Glass Manufacturing* **2020**, *1* (4). Published within *ACerS Bulletin 99* (7), 54−58.

(33) Hassan, K.; Nine, M. J.; Tung, T. T.; Stanley, N.; Yap, P. L.; Rastin, H.; Yu, L.; Losic, D. Functional inks and extrusion-based 3D printing of 2D materials: a review of current research and applications. *Nanoscale* **2020**, *12*, 19007−19042.

(34) Kim, M. J.; Cruz, M. A.; Chen, Z.; Xu, H.; Brown, M.; Fichthorn, K. A.; Wiley, B. J. Isotropic Iodide Adsorption Causes Anisotropic Growth of Copper Microplates. *Chem. Mater.* **2021**, *33*, 881−891.

(35) Kim, M. J.; Alvarez, S.; Yan, T.; Tadepalli, V.; Fichthorn, K. A.; Wiley, B. J. Modulating the Growth Rate, Aspect Ratio, and Yield of Copper Nanowires with Alkylamines. *Chem. Mater.* **2018**, *30*, 2809−2818.

(36) Nanda, K. K. Size-dependent melting of nanoparticles: Hundred years of thermodynamic model. *Pramana − J. Phys.* **2009**, *72*, 617−628.

(37) Zhang, M.; Efremov, M. Y.; Schiettekatte, F.; Olson, E.; Kwan, A.; Lai, S.; Wisleder, T.; Greene, J.; Allen, L. Size-dependent melting point depression of nanostructures: Nanocalorimetric measurements. *Phys. Rev. B* **2000**, *62*, No. 10548.

(38) Chutia, A.; Silverwood, I. P.; Farrow, M. R.; Scanlon, D. O.; Wells, P. P.; Bowker, M.; Parker, S. F.; Catlow, C. R. A. Adsorption of formate species on Cu(h,k,l) low index surfaces. *Surf. Sci.* **2016**, *653*, 45−54.

(39) Hidalgo-Manrique, P.; Lei, X.; Xu, R.; Zhou, M.; Kinloch, I. A.; Young, R. J. Copper/graphene composites: a review. *J. Mater. Sci.* **2019**, *54*, 12236−12289.

(40) Subramaniam, C.; Yamada, T.; Kobashi, K.; Sekiguchi, A.; Futaba, D. N.; Yumura, M.; Hata, K. One hundred fold increase in current carrying capacity in a carbon nanotube−copper composite. *Nat. Commun.* **2013**, *4*, No. 2202.

(41) Okpalugo, T. I. T.; Papakonstantinou, P.; Murphy, H.; McLaughlin, J.; Brown, N. M. D. High resolution XPS characterization of chemical functionalised MWCNTs and SWCNTs. *Carbon* **2005**, *43*, 153−161.

(42) Johra, F. T.; Lee, J.-W.; Jung, W.-G. Facile and safe graphene preparation on solution based platform. *J. Ind. Eng. Chem.* **2014**, *20*, 2883−2887.

(43) Li, Q.; Pan, H.; Higgins, D.; Cao, R.; Zhang, G.; Lv, H.; Wu, K.; Cho, J.; Wu, G. Metal−Organic Framework-Derived Bamboo-like Nitrogen-Doped Graphene Tubes as an Active Matrix for Hybrid Oxygen-Reduction Electrocatalysts. *Small* **2015**, *11*, 1443−1452.

(44) Efimov, A. A.; Arsenov, P. V.; Borisov, V. I.; Buchnev, A. I.; Lizunova, A. A.; Kornyushin, D. V.; Tikhonov, S. S.; Musaev, A. G.; Urazov, M. N.; Shcherbakov, M. I.; Spirin, D. V.; Ivanov, V. V. Synthesis of Nanoparticles by Spark Discharge as a Facile and Versatile Technique of Preparing Highly Conductive Pt Nano-Ink for Printed Electronics. *Nanomaterials* **2021**, *11*, No. 234.

(45) Gao, Y.; Li, H.; Liu, J. Direct Writing of Flexible Electronics through Room Temperature Liquid Metal Ink. *PLoS One* **2012**, *7*, No. e45485.

(46) Khan, S.; Nguyen, T. P.; Lubej, M.; Thiery, L.; Vairac, P.; Briand, D. Low-power printed micro-hotplates through aerosol jetting of gold on thin polyimide membranes. *Microelectron. Eng.* **2018**, *194*, 71−78.

(47) Shirai, H.; Nguyen, M. T.; Ishida, Y.; Yonezawa, T. A new approach for additive-free room temperature sintering of conductive patterns using polymer-stabilized Sn nanoparticles. *J. Mater. Chem. C* **2016**, *4*, 2228−2234.

(48) Kim, T. G.; Park, H. J.; Woo, K.; Jeong, S.; Choi, Y.; Lee, S. Y. Enhanced Oxidation-Resistant Cu@Ni Core−Shell Nanoparticles for Printed Flexible Electrodes. *ACS Appl. Mater. Interfaces* **2018**, *10*, 1059−1066.

(49) Secor, E. B.; Prabhumirashi, P. L.; Puntambekar, K.; Geier, M. L.; Hersam, M. C. Inkjet Printing of High Conductivity, Flexible Graphene Patterns. *J. Phys. Chem. Lett.* **2013**, *4*, 1347−1351.

(50) Yu, F.; Wang, K.; Liu, J.; Fu, X.; Chen, H.; Li, M. Ag-Sn bimetallic nanoparticles paste for high temperature service in power devices. *Nanotechnology* **2020**, *31*, No. 345204.

(51) Data acquired from Creative Materials for product # 101-42 (Ag), 107-25 (C), and 107-40 (Ni) at http://www.creativematerials.com/data-sheets/.